

# Interplay between Kondo suppression and Lifshitz transitions in $\text{YbRh}_2\text{Si}_2$ at high magnetic fields

H. Pfau,<sup>1</sup> R. Daou,<sup>1,2</sup> S. Lausberg,<sup>1</sup> H. R. Naren,<sup>1</sup> M. Brando,<sup>1</sup> S. Friedemann,<sup>1,3</sup> S. Wirth,<sup>1</sup>  
T. Westerkamp,<sup>1</sup> U. Stockert,<sup>1</sup> P. Gegenwart,<sup>1,\*</sup> C. Krellner,<sup>1,†</sup> C. Geibel,<sup>1</sup> G. Zwirgagl,<sup>4</sup> and F. Steglich<sup>1</sup>

<sup>1</sup>*Max Planck Institute for Chemical Physics of Solids, D-01187 Dresden, Germany*

<sup>2</sup>*Laboratoire CRISMAT, UMR 6508 du CNRS, ENSICAEN et Université de Caen, F-14050 Caen, France.*

<sup>3</sup>*Cavendish Laboratory, University of Cambridge, Cambridge CB3 0HE, UK*

<sup>4</sup>*Institut für Mathematische Physik, Technische Universität Braunschweig, D-38106 Braunschweig, Germany*

(Dated: February 28, 2013)

We investigate the magnetic field dependent thermopower, thermal conductivity, resistivity and Hall effect in the heavy fermion metal  $\text{YbRh}_2\text{Si}_2$ . In contrast to reports on thermodynamic measurements, we find in total three transitions at high fields, rather than a single one at 10 T. Using the Mott formula together with renormalized band calculations, we identify Lifshitz transitions as their origin. The predictions of the calculations show that all experimental results rely on an interplay of a smooth suppression of the Kondo effect and the spin splitting of the flat hybridized bands.

Since their discovery almost four decades ago, Kondo lattice systems pose a challenge to condensed-matter physicists. Above the characteristic Kondo temperature  $T_K$  they contain a periodic lattice of local  $4f$ -derived paramagnetic moments. Below  $T_K$ , these moments become reduced and eventually fully screened by the conduction electrons: The entanglement of the localized  $4f$  states with the delocalized conduction-band states leads to the formation of local Kondo singlets, which develop weak dispersion as a consequence of their periodic arrangement (Bloch's theorem) [1]. The delocalized Kondo singlets act as (composite) charge carriers, which exhibit a large effective mass (heavy fermions) due to the extremely strong on-site Coulomb correlations. This is inferred from a huge Sommerfeld coefficient of the electronic specific heat [2] but is invisible, *e.g.*, in photoelectron spectroscopy [3], probing one-electron properties. The localized  $4f$  states at  $T > T_K$  are not part of the “small” Fermi surface (FS). However, being constituent to the composite charge carriers, the delocalized  $4f$  states do contribute to a “large” FS below  $T_K$ .

Recently, the effect of a magnetic field on these composite fermions has become an important issue. On the one hand most of the information on these quasiparticles comes from de Haas van Alphen (dHvA) experiments performed at high fields. However, band structure calculations, necessary to analyze these experimental results, exist almost exclusively at zero field [4, 5]. On the other hand, many heavy fermion systems undergo a metamagnetic transition at fields of the order of 10 T [6–9], where in some cases direct evidence (from dHvA) for a change of the FS and thus, of the heavy quasiparticles has been found [5, 10], the origin of which remains controversial.

$\text{YbRh}_2\text{Si}_2$  is such a case: Specific heat, susceptibility and magnetostriction measurements revealed anomalies at a critical field  $B_0 = 10$  T, indicating a rapid decrease of the effective mass at  $B_0$  [9, 11, 12]. This was initially interpreted as a breakdown of the Kondo screening

resulting in a small FS on the high field side. Later, dHvA experiments were interpreted in terms of a Lifshitz transition at  $B_0$ , where a spin-split band disappears [5, 13]. While these two interpretations seem quite different at first sight, they essentially rely on a similar model: Only in the presence of the very flat bands of the composite fermions, the Zeeman splitting can induce such large effects on the FS at moderate fields as observed in  $\text{YbRh}_2\text{Si}_2$ . Simultaneously a splitting also drives the “large” FS continuously toward the “small” one and leads to a decrease of the quasiparticle mass. Therefore, the field scale for both processes is related to  $T_K$ .

In order to get more insight into the field evolution of the quasiparticles and into the connection between destruction of the composite fermions and the occurrence of Lifshitz transitions, we performed detailed, field dependent transport studies in  $\text{YbRh}_2\text{Si}_2$  in fields to at least 12 T. We focus on the effects far above the quantum critical point (QCP) at  $B = 0.06$  T which shall not be addressed here. In contrast to reports on thermodynamic measurements [9, 11, 12], we show that the transition at  $B_0$  consists of two close-lying features. Moreover, we observe an additional transition at 3.4 T. From the remarkable agreement between thermopower, electrical conductivity and magnetostriction above 2 T within the framework of Mott's formula, we demonstrate that all three transitions are caused by band structure effects.

We compare our experimental results with predictions of the renormalized band (RB) structure calculation. They reveal three successive Lifshitz transitions at the three experimentally observed transition fields. This agreement demonstrates that the observed field evolution results from an interplay of a smooth suppression of the Kondo effect and the spin splitting of a sharply structured density of states (DOS) generated by a strong anisotropic hybridization.

We investigated three high quality samples from the same batch, with a residual resistivity of approximately

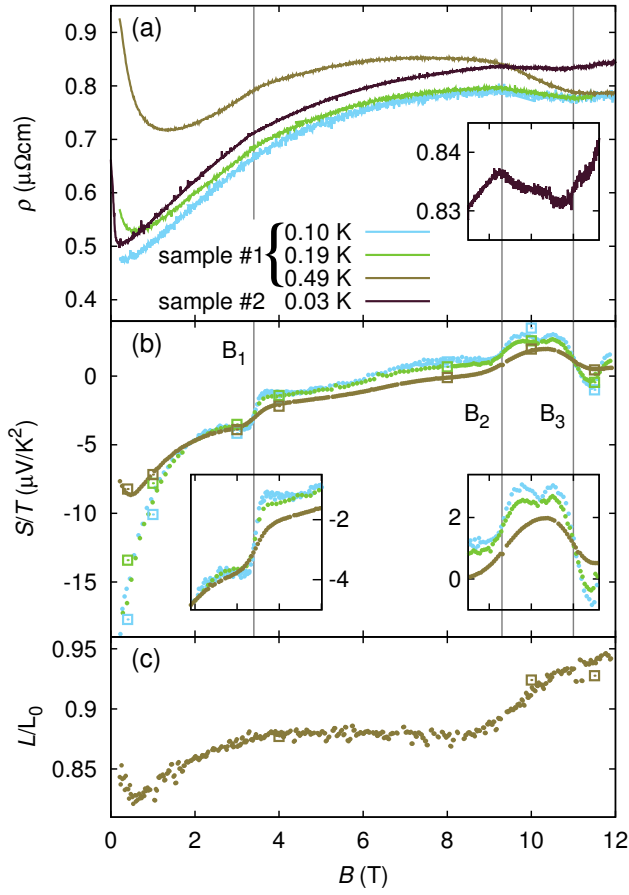


FIG. 1. Magnetoresistance,  $\rho$ , thermopower,  $S/T$ , and Lorenz ratio,  $L/L_0$  plotted as a function of magnetic field  $B$ . Lines and dots denote field sweeps, open squares are extracted from temperature sweeps. (a)  $\rho$  shows three kinks at  $B_1 = 3.4$  T,  $B_2 = 9.3$  T and  $B_3 = 11.0$  T. Their position is sample- and temperature-independent. Inset: enlarged view for 0.03 K. (b)  $S/T$  of sample #1 at the same temperatures as in (a). The complex behaviour with several zero crossings reflects the multi-band character of YbRh<sub>2</sub>Si<sub>2</sub>. All three transitions are characterised by pronounced steps (insets: enlarged view). (c) The Lorenz ratio at 0.49 K is below unity with a minimum at about 0.5 T.

0.5  $\mu\Omega\text{cm}$ . On sample #1 we performed simultaneous d.c. resistivity, thermal conductivity and thermopower measurements down to 0.1 K and for  $0.2 \text{ T} \leq B \leq 12 \text{ T}$  using the same soldered contacts, as described in Ref. 14. Sample #2 was used to extend the resistivity data down to 0.03 K on another set-up applying an a.c. technique. We also performed Hall-effect measurements on sample #3 down to 0.05 K and up to 15 T. The magnetic field  $B$  was always applied perpendicular to the  $c$ -axis. The currents for resistivity and thermal transport were parallel to  $B$ , for the Hall-effect perpendicular to  $c$  and  $B$ .

Figures 1(a) and 1(b) show the low-temperature magnetoresistivity  $\rho(B)$  and the isothermal, field-dependent

thermopower  $S(B)$ , respectively. The Lorenz ratio  $L(B)/L_0 = \kappa(B)\rho(B)/TL_0$  obtained from magnetoresistance and thermal conductivity  $\kappa$  using Sommerfeld's constant  $L_0 = \pi^2 k_B^2/3e^2$ , is shown in Fig. 1(c) only for 490 mK, because of an enhanced noise level at lower temperatures. Considering the  $B$ - $T$  phase diagram of YbRh<sub>2</sub>Si<sub>2</sub> [9], it is natural to relate the low-field ( $B < 2$  T) behaviour of all these quantities to the signatures of the QCP and the surrounding non-Fermi liquid regime. Since our field range for the measurements on sample #1 is limited to above 0.2 T, we observe only the high-field branch of these signatures, which extends to roughly 2 T. Nevertheless, our measurements agree with previously reported results: the step in magnetoresistance [15], the pronounced minimum in  $S(B)/T$  [16] and the minimum of the isothermal Lorenz ratio [17] are clearly visible.

Next, we focus on the high-field properties beyond 2 T, where YbRh<sub>2</sub>Si<sub>2</sub> is a Fermi liquid below 200 mK [9]. The key features are three transitions visible as tiny kinks in the magnetoresistance at  $B_1 = (3.4 \pm 0.1)$  T,  $B_2 = (9.3 \pm 0.1)$  T and  $B_3 = (11.0 \pm 0.2)$  T in Fig. 1(a). The transitions are more obvious in the thermopower (Fig. 1(b)):  $S(B)/T$  shows three pronounced steps, which become sharper at lower  $T$ .

These observations are interesting from two perspectives. Firstly, previous measurements have not observed features at 3.4 T [9, 11, 12]. And secondly, the transition reported in magnetisation, specific heat and magnetostriction [9, 11, 12] at roughly 10 T is actually composed of two well-separated features at 9.3 T and 11.0 T down to 30 mK, which do not merge in the extrapolation  $T \rightarrow 0$ .

We further analyse our data using the Mott formula [18] for the diffusion thermopower to clarify if the observed features have a thermodynamic origin. Phonon drag contributions to the thermopower are negligible in this temperature range [19]. The Mott formula generally holds at low temperatures in the absence of inelastic scattering [20]. To expand it, we first exchange the energy derivative of  $\ln \sigma$  with the field derivative using  $\partial B/\partial \epsilon$ . In the second step, we use  $\sigma = ne^2\tau/m^*$  together with  $m^* \propto N^{2/3}$  (in 3D) and obtain

$$\frac{S}{eL_0T} = \frac{\partial B}{\partial \epsilon} \frac{\partial \ln \sigma}{\partial B} \Big|_{\epsilon_F} = \frac{\partial B}{\partial \epsilon} \left( \frac{\partial \ln \tau}{\partial B} - \frac{2}{3} \frac{\partial \ln N}{\partial B} \right)_{\epsilon_F} \quad (1)$$

where  $\sigma = 1/\rho$  is the electrical conductivity,  $n$  the total electron concentration,  $N$  the DOS,  $m^*$  the effective mass, and  $\tau$  the scattering time. This splits the thermopower into a scattering part ( $\tau$ ) and a part representing the band structure ( $N$ ).

To test the first expansion in Equation 1, we compare  $S(B)/T$  with  $\partial \ln \sigma/\partial B$  in Fig. 2(a). Above 3 T, both curves can be scaled on top of each other using a constant  $\partial B/\partial \epsilon$ . This suggests a linear relationship between

$\epsilon$  and  $B$ , which we write in terms of an effective Zeeman energy  $\epsilon = g_{\text{eff}}\mu_B B/2$ , with  $g_{\text{eff}}$  of  $16 \pm 1$  ( $\mu_B$  is the Bohr magneton), and discuss later on. Moreover, it implies that inelastic scattering (which would invalidate the Mott formula) is insignificant in this regime. In the low-field region below 2 T both curves show a disparate behaviour. Consequently either  $\epsilon \propto B$  is violated or inelastic scattering is significant. Both are likely to occur close to a QCP: The first can arise if there are dramatic changes in the magnetisation, the band structure or the FS. Inelastic scattering can increase close to a phase transition.

We now turn to the second expansion of Equation 1 and use the linear magnetostriction coefficient  $\lambda$  as a thermodynamic probe to access the contribution from the DOS, since the data available have a higher resolution than *e.g.* specific heat or magnetisation. The inset in Fig. 2(b) demonstrates that the linear magnetostriction ( $\Delta l \parallel B \perp c$ ) follows  $\Delta l/l \propto M^{2.7}$  over the entire field range. In a Fermi liquid  $\chi = \partial M/\partial B$  follows the behaviour of the DOS, and therefore also does  $\lambda = \partial(\Delta l/l)/\partial B$ . Applying a constant scaling factor,  $\partial \ln \lambda/\partial B$  matches  $S/T$  in Fig. 2(b), even at low fields. Only the double hump around 10 T is more pronounced. Considering the nice agreement of  $S$  and  $\sigma$  in the same low-field regime is due to enhanced inelastic scattering rather than a failure of  $\epsilon \sim B$ . The surprisingly good qualitative agreement, especially at  $B_1$ ,  $B_2$  and  $B_3$ , is clear evidence that the origin of all three transitions lies within the correlated band structure of  $\text{YbRh}_2\text{Si}_2$ .

Our experimental data together with previous results already indicate the complex nature of these band structure effects. For example, the transition around  $B_0$  is composed of two fields and the drop in the specific heat coefficient  $\gamma(B)$  between them is only moderate with a decrease from about 250 mJ/molK<sup>2</sup> to 100 mJ/molK<sup>2</sup>. It is therefore unlikely that either a single Lifshitz transition [5] or a sudden localization of the  $f$ -electrons [9, 11, 12] is—on its own—a sufficient model to describe the behaviour around 10 T. Hence, a theory of the field evolution of  $\text{YbRh}_2\text{Si}_2$  should include not only the Kondo effect to describe de-renormalization processes, but also the specific correlated band structure of  $\text{YbRh}_2\text{Si}_2$  to reveal topological transitions.

We therefore conducted the field-dependent RB calculations summarized in Fig. 3, which are an extension to the results from Ref. 21 with a focus on the detailed development of the FS and the DOS in field. We used the RB method described in Ref. 21 and 22 with a very tight  $k$ -mesh in zero field of 8125 points in the irreducible wedge to resolve changes in the isoenergy surfaces. In finite fields we used 405  $k$ -points.

Figure 3(a) shows the calculated zero-field quasiparticle DOS  $N(\epsilon)$  and Fig. 3(b) displays the corresponding isoenergy surfaces of the most important FS sheets

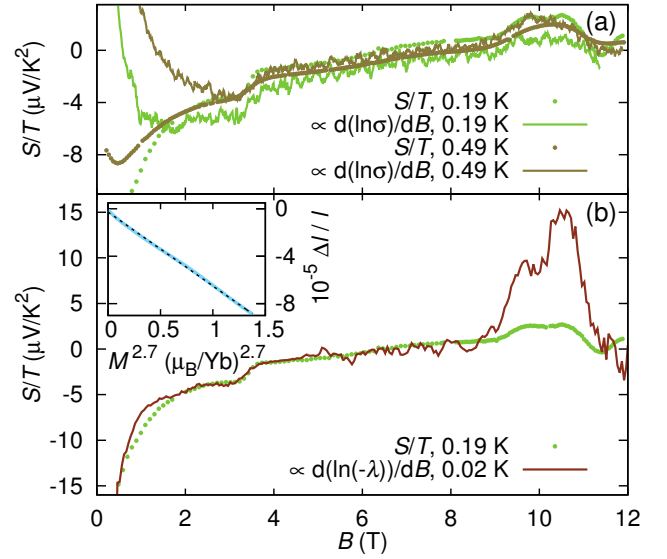


FIG. 2. Analysis of the thermopower with the Mott formula. The measured  $S/T$  (dots) is compared with that calculated (lines) from (a) the electrical conductivity and from (b) the magnetostriction coefficient using Equation 1 with  $\partial \ln N/\partial B \propto \partial \ln \lambda/\partial B$  and  $\partial \ln \tau/\partial B = 0$ . Within the Fermi liquid regime ( $B > 2 - 3$  T) all curves show the same overall behaviour. Inset: Magnetisation dependence of the magnetostriction. The data (solid blue) perfectly follows a power law  $\Delta l/l \propto M^{2.7}$  (dashed black line).

with  $f$ -character—the so called “doughnut” (top) and the “jungle gym” (bottom), respectively. Scanning through  $N(\epsilon)$  within the displayed energy range, the calculations predict the four color-coded regimes characterized by different topologies of the isoenergy surfaces, separated by Lifshitz transitions.

An applied magnetic field spin splits the DOS into a minority and a majority branch. These do not shift rigidly in field but the amplitude of the coherence peak decreases (Fig. 3(c)), mainly because of the weakening of the Kondo effect. Nevertheless the characteristics of the band structure are not changed. Therefore we expect the energy evolution of the isoenergy surfaces in Fig. 3(b) to be the same as the field evolution of the FS. *I.e.*, the FS of the majority band stays in the red (D) regime, while the FS topology of the minority band changes from the red (D) type through yellow (C) and green (B) to the one marked in blue (A).

We take advantage of the similar shape of the zero- and finite-field DOS and assign the energy of a topology change (in zero field) to a magnetic field where the corresponding feature in the DOS crosses  $\epsilon_F$ : The transition from the blue (A) to the green (B) regime corresponds to a kink in the DOS which reaches  $\epsilon_F$  for  $\tilde{B}_3 = (11 \pm 1)$  T. Similarly, we obtain  $\tilde{B}_2 = (9 \pm 1)$  T for the second transition (green (B) - yellow (C)). The difference  $\tilde{B}_3 - \tilde{B}_2$  fits

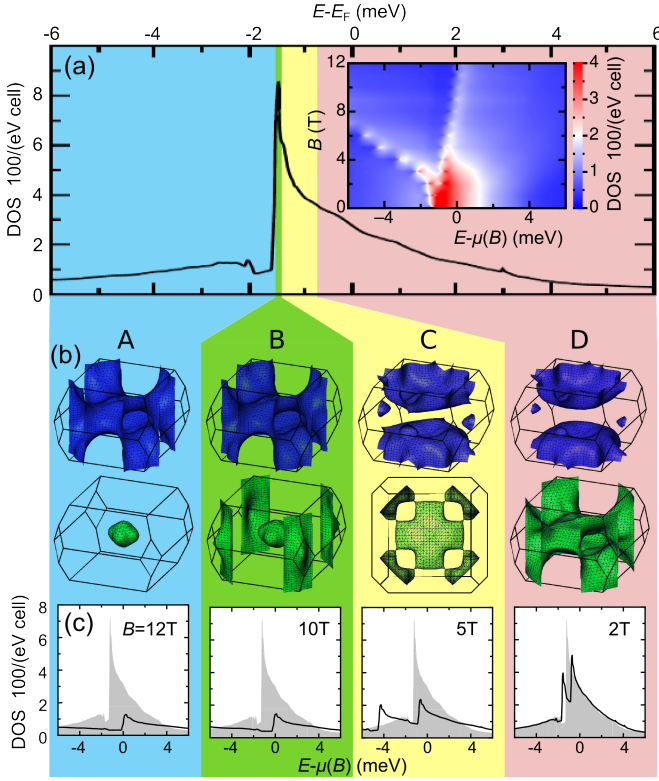


FIG. 3. Isoenergy surfaces for  $B = 0$  and the quasiparticle DOS development in finite field calculated using the RB method. The zero-field DOS in (a) is divided into four regions (blue (A), green (B), yellow (C), red (D)) distinguished by different topologies of the isoenergy surfaces shown in (b). In the yellow region (C), we show in plan the “jungle gym” FS sheet exactly at the topological transition between B and C. (c) illustrates the magnetic field evolution of the DOS for selected fields, with the zero-field DOS in grey for comparison. Inset in (a): Energy-field map of the DOS interpolated in 1 T steps. One can assign the four energy regions and their isoenergy surfaces in a) and b) to the four field ranges and their FS separated by  $\tilde{B}_1$ ,  $\tilde{B}_2$  and  $\tilde{B}_3$ .

to the linear shift of 0.1 meV/T (inset Fig. 3(a)), which in turn matches the ESR  $g$ -factor of 3.5 [23] (applying  $\tilde{\epsilon} = g\mu_B B/2$ ). We use this shift to estimate the field corresponding to the weak third transition from yellow (C) to red (D) to  $\tilde{B}_1 = (2.5 \pm 1)$  T. These fields, extracted from the calculations, are in excellent agreement with the transitions  $B_1$ ,  $B_2$  and  $B_3$  found in the experiment. This proves that they correspond to three Lifshitz transitions of the types illustrated in Fig. 3(b).

Additionally, the linear sweep of the van-Hove singularity predicted by our calculations confirms the linear energy-field dependence found in our data analysis. It is worth reiterating that the only adjustable parameter leading to the remarkable accuracy of the Mott formula in the two comparisons shown in Fig. 2 is  $g_{\text{eff}}$ . Moreover, the thermopower as well as  $\partial \ln \lambda / \partial B$  and  $\partial \ln \sigma / \partial B$  are

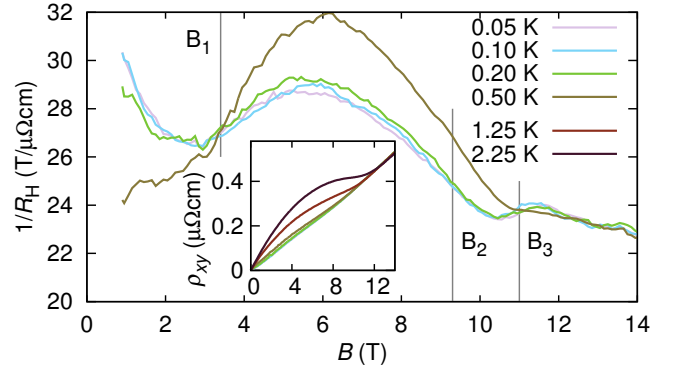


FIG. 4. Hall effect on sample #3. The field-dependent inverse Hall coefficient shows several extrema close to  $B_1, B_2$  and  $B_3$  obtained from resistivity data (see Fig. 1(a)). Inset: the Hall resistivity,  $\rho_{xy}$ , is almost linear below 0.2 K.

independent of sample geometry, thus systematic errors are almost negligible. The difference between  $g_{\text{eff}} = 16$  (corresponding to a  $\partial \epsilon / \partial B = 0.5$  meV/T) and  $g = 3.5$  (0.1 meV/T) from our calculations, however, is unsurprising, since a rigid band shift is obviously insufficient to account for the experimental data. Unexpectedly, these field-induced changes of the band structure also enter linearly into  $g_{\text{eff}}$ , a fact which certainly deserves further studies.

Our results confirm on the one hand that the Fermi liquid state observed in  $\text{YbRh}_2\text{Si}_2$  in finite magnetic fields originates from the formation of local Kondo singlets. A magnetic field suppresses the local Kondo effect. However, Numerical Renormalization Group method for a single impurity (see *e.g.* [24–27]) predicts a continuous decrease of the effective mass. Therefore, our calculations demonstrate on the other hand that the single impurity model alone cannot account for the abrupt changes in the observed quantities reported here. The latter have to be attributed to coherence effects arising from the periodic arrangement of the Kondo ions. The anisotropic hybridization of the  $4f$  states with the conduction bands, caused by the highly anisotropic crystalline electric field (CEF) ground state, leads to van-Hove-type singularities in the quasiparticle DOS. The structures in the quasiparticle DOS highlight changes of the iso-energy surfaces as shown in Fig. 3. In a magnetic field, the  $4f$  states are split which, in turn, leads to a Zeeman splitting of the quasiparticle bands. The relative shifts of the latter, however, are enhanced by a field-dependent Sommerfeld-Wilson ratio which reflects the local many-body effects.

Experimentally, further insight into the evolution of the FS can be obtained by Hall effect measurements. The isothermal Hall resistivity  $\rho_{xy}(B)$  for selected  $T$  is presented in the inset of Fig. 4 and indicates hole-dominated transport. Importantly, beyond 12 T all curves coincide pointing towards a field-driven suppression of the local

Kondo effect. This suppression is a continuous process and likely accounts for the maximum in the effective carrier concentration,  $1/R_H = 1/\frac{d\sigma_{xy}}{dB}$ , at around 6 T and lowest temperatures via the hybridization of conduction and  $4f$  electrons. For  $T > 0.2$  K an anomalous contribution [28] to  $R_H$  comes into play (*cf.* also [29]) such that  $1/R_H$  no longer tracks the carrier concentration. Qualitatively, the transitions at  $B_1$ ,  $B_2$  and  $B_3$  are observed as extrema in  $R_H(B)$  although—quantitatively—at slightly different fields. The latter might be caused by the complex nature of the Hall effect [30] (*e.g.* multiple bands) or the different current alignment  $j \perp B$  ( $j \parallel B$  for all other measurements).

In conclusion, we showed that the thermopower is an excellent tool to reveal field induced changes in the FS of a correlated metal, hardly detectable by any other probe. In  $\text{YbRh}_2\text{Si}_2$ , we find three successive transitions, which were identified as Lifshitz transitions by a comparison with predictions from detailed RB calculations. This implies, that the unusual high-field properties of  $\text{YbRh}_2\text{Si}_2$  arise from the interplay of (a) the symmetry of the CEF ground state (g-factor, anisotropic hybridization), (b) the suppression of the local Kondo effect (reduced effective mass, field-dependent Sommerfeld-Wilson ratio) and (c) the coherence effects due to the periodicity of the lattice (van-Hove singularities, Lifshitz transitions). The excellent agreement between our experimental results and our RB calculations demonstrates that RB calculations are a very suitable approach to describe quasiparticles in the Kondo lattice.

We acknowledge insightful discussions with F. F. Assad and M. Bercx. Part of this work has been supported by the DFG Research Unit 960 Quantum Phase Transitions.

---

\* I. Physikalisches Institut, Georg-August-Universität Göttingen, D-37077 Göttingen, Germany

† Physikalisches Institut, Johann Wolfgang Goethe-Universität, D-60438 Frankfurt am Main, Germany

- [1] A. C. Hewson, *The Kondo Problem to Heavy Fermions* (Cambridge University Press, Cambridge, 1993).
- [2] O. Trovarelli, C. Geibel, S. Mederle, C. Langhammer, F. M. Grosche, P. Gegenwart, M. Lang, G. Sparn, and F. Steglich, *Phys. Rev. Lett.* **85**, 626 (2000).
- [3] K. Kummer, Yu. Kucherenko, S. Danzenbächer, C. Krellner, C. Geibel, M. G. Holder, L. V. Bekenov, T. Muro, Y. Kato, T. Kinoshita, S. Huotari, L. Simonelli, S. L. Molodtsov, C. Laubschat and D. V. Vyalikh, *Phys. Rev. B* **84**, 245114 (2011).
- [4] K. Miyake and H. Ikeda, *J. Phys. Soc. Jpn.* **75**, 033704 (2006).
- [5] P. Rourke, A. McCollam, G. Lapertot, G. Knebel, J. Flouquet, and S. Julian, *Phys. Rev. Lett.* **101**, 237205 (2008).
- [6] P. Haen, J. Flouquet, F. Lapierre, P. Lejay, and G. Remenyi, *J. Low Temp. Phys.* **67**, 391 (1987).
- [7] M. Deppe, S. Lausberg, F. Weickert, M. Brando, Y. Skourski, N. Caroca-Canales, C. Geibel, and F. Steglich, *Phys. Rev. B* **85**, 060401 (2012).
- [8] A. Schröder, H. G. Schlager, and H. v. Löhneysen, *J. Magn. Magn. Mat.* **108**, 47 (1992).
- [9] P. Gegenwart, Y. Tokiwa, T. Westerkamp, F. Weickert, J. Custers, J. Ferstl, C. Krellner, C. Geibel, P. Kersch, K.-H. Müller, and F. Steglich, *New J. Phys.* **8**, 171 (2006).
- [10] H. Aoki, S. Uji, A. K. Albessard, and Y. Ōnuki, *Phys. Rev. Lett.* **71**, 2110 (1993).
- [11] Y. Tokiwa, P. Gegenwart, F. Weickert, R. Küchler, J. Custers, J. Ferstl, C. Geibel, and F. Steglich, *J. Magn. Magn. Mater.* **272-276**, e87 (2004).
- [12] Y. Tokiwa, P. Gegenwart, T. Radu, J. Ferstl, G. Sparn, C. Geibel, and F. Steglich, *Phys. Rev. Lett.* **94**, 226402 (2005).
- [13] I. Lifshitz, *Soviet Physics JETP* **11**, 1130 (1960).
- [14] H. Pfau, R. Daou, M. Brando, and F. Steglich, *Phys. Rev. B* **85**, 035127 (2012).
- [15] P. Gegenwart, T. Westerkamp, C. Krellner, Y. Tokiwa, S. Paschen, C. Geibel, F. Steglich, E. Abrahams, and Q. Si, *Science* **315**, 969 (2007).
- [16] S. Hartmann, N. Oeschler, C. Krellner, C. Geibel, S. Paschen, and F. Steglich, *Phys. Rev. Lett.* **104**, 096401 (2010).
- [17] H. Pfau, S. Hartmann, U. Stockert, P. Sun, S. Lausberg, M. Brando, S. Friedemann, C. Krellner, C. Geibel, S. Wirth, S. Kirchner, E. Abrahams, Q. Si, and F. Steglich, *Nature* **484**, 493 (2012).
- [18] N. F. Mott and E. A. Davis, *Electronic processes in non-crystalline materials*, Oxford Univ. Press, Oxford (1971).
- [19] S. Hartmann, Ph.D. thesis, Technische Universität Dresden, 2010.
- [20] M. Johnson, and G. Mahan, *Phys. Rev. B* **21**, 4223 (1980).
- [21] G. Zwircknagl, *J. Phys. Condens. Matter* **23**, 094215 (2011).
- [22] G. Zwircknagl, *Adv. Phys.* **41**, 203 (1992).
- [23] U. Schaufuß, V. Kataev, A. A. Zvyagin, B. Büchner, J. Sichelschmidt, J. Wykoff, C. Krellner, C. Geibel, and F. Steglich, *Phys. Rev. Lett.* **102**, 076405 (2009).
- [24] J. Bauer, and A. C. Hewson, *Phys. Rev. B*, **76**, 035119 (2007).
- [25] A. C. Hewson, and J. Bauer, W. Koller, *Phys. Rev. B*, **73**, 045117 (2006).
- [26] A. C. Hewson, A. Oguri, and D. Meyer, *Eur. Phys. J. B*, **40**, 177 (2004).
- [27] R. Peters, T. Pruschke, and F. B. Anders, *Phys. Rev. B*, **74**, 245114 (2006).
- [28] P. Coleman, P. W. Anderson, and T. V. Ramakrishnan, *Phys. Rev. Lett.* **55**, 414 (1985).
- [29] S. Paschen, T. Lühmann, S. Wirth, P. Gegenwart, O. Trovarelli, C. Geibel, F. Steglich, P. Coleman, and Q. Si, *Nature* **432**, 881 (2004).
- [30] S. Nair, S. Wirth, S. Friedemann, F. Steglich, Q. Si and A. J. Schofield, *Adv. Phys.* **61**, 583 (2012).